Soft Matter

Accepted Manuscript

This is an *Accepted Manuscript*, which has been through the Royal Society of Chemistry peer review process and has been accepted for publication.

Accepted Manuscripts are published online shortly after acceptance, before technical editing, formatting and proof reading. Using this free service, authors can make their results available to the community, in citable form, before we publish the edited article. We will replace this *Accepted Manuscript* with the edited and formatted *Advance Article* as soon as it is available.

You can find more information about *Accepted Manuscripts* in the Information for Authors.

Please note that technical editing may introduce minor changes to the text and/or graphics, which may alter content. The journal's standard Terms & Conditions and the Ethical guidelines still apply. In no event shall the Royal Society of Chemistry be held responsible for any errors or omissions in this *Accepted Manuscript* or any consequences arising from the use of any information it contains.

ROYAL SOCIETY OF CHEMISTRY

www.rsc.org/softmatter

Aβ Self-Association and Adsorption on a Hydrophobic Nanosurface: Competitive Effects and the Detection of Small Oligomers via Electrical Response

Asis K. Jana and Neelanjana Sengupta*

Physical Chemistry Division, CSIR-National Chemical Laboratory, Pune 411008, India

Soft Matter Accepted Manuscript

* Correspondence: n.sengupta@ncl.res.in

ABSTRACT

Treatment of Alzheimer's disease (AD) is impeded by lack of effective early diagnostic methods. Small, soluble Aβ globulomers play a major role in AD neurotoxicity, and detecting their presence in aqueous fluids could lead to suitable sensors. We evaluate adsorption behavior of small Aβ oligomers on the surface of a single walled carbon nanotube of high curvature. While the intrinsic self-assembly propensity of Aβ is markedly hindered by adsorption, the oligomeric units show high degrees of surface immobilization. Immobilized complexes are capable of oligomeric growth, but with a shifted monomer-oligomer equilibrium compared to the free states. In presence of an ionic solution and suitable external electric fields, magnitudes of the current blockades are found to be sensitive to the oligomeric number of the adsorbed complex. However, this sensitivity gradually diminishes with increasing oligomeric size. The results provide a proof-of-concept basis for further investigations in the design of sensors for detecting the toxic small oligomers of Aβ.

Soft Matter Accepted Manuscript

1. Introduction

The profound influence of nanomaterials on the behavior of intrinsically disordered proteins (IDPs) has come to the fore recently.[1-3] IDPs defy the classic protein structure-function paradigm in biology.[4] Importantly, their inherent resistance to adopt natively folded forms can be compensated by their high tendency to form self-assembled units, which are often associated with the onset of debilitating neurodegenerative diseases.[5, 6] Key insights into IDP self-assembly pathways have emerged over the last decade from a combination of advanced experimental, theoretical and computational approaches.[7-13] It is believed that the underlying physico-chemical basis of nanomaterial influence on IDP assembly could be harnessed for potential therapeutic and diagnostic applications in combating these debilitating proteopathies.[1,14-16]

The 4 kDa Amyloid beta (Aβ) peptide, often considered a paradigm for studying IDP self-assembly, is associated with familial as well as sporadic Alzheimer's disease (AD).[17] AD has no cure yet, and its prognosis is worsened by a lack of early diagnostic methods. Aβ assembly can be described as a nucleation dependent process wherein the formation of a critical nucleus triggers higher ordered growth characterized by the appearance of insoluble amyloid fibrils.[18,19] It is noteworthy, however, that recent research implicates soluble small oligomers of Aβ, rather than its fibrillar aggregates, in AD neurotoxicity.[20-22] A detailed molecular picture of the early oligomeric self-assembly pathway is therefore necessary to design effective AD therapeutics. But the tendency of the Aβ monomer to aggregate very rapidly in water hinders experiments designed to probe mechanistic aspects of the assembly pathways.[23,24] However, structural information on the monomeric and various self-assembled forms has been obtained via NMR methods.[25] In this respect, computational and theoretical methods have been indispensable in the development of mechanistic models for the Aβ

Soft Matter Accepted Manuscript

aggregation process and in unraveling roles of key domains within the peptide sequence.[7,18,26-30]

Non-covalent interactions arising from various nanomaterials could be harnessed for modulating the intrinsic self-assembly characteristics of Aβ. Interactions of Aβ with polymeric, gold, or TiO_2 nanoparticles may potentially enhance fibrillation rates, as suggested by a growing body of *in vitro* research.[31-34] Conversely, carbon nanomaterials such as fullerene, carbon nanotubes and graphene oxide have been shown to strongly influence conformational properties in Aβ units, destabilize Aβ protofibrils, and reduce the size of the aggregates in a concentration dependent manner.[35-39] Kim and Lee first showed that 1,2-(dimethoxylmethano) fullerene specifically binds to KLVFF region of Aβ protein, thereby suppressing Aβ aggregation.[40] More recently, Andujar *et al.* found that fullerene (C_{60}) can preferentially bind to the turn region of pentameric Aβ and destabilize the intramolecular and intermolecular salt bridges.[38] Mahmoudi *et al.* have recently reported that graphene oxide can increase lag phase of Aβ fibrillation process through adsorption of Aβ monomers.[41] Li *et al.* found that single walled carbon nanotubes (SWCNT) inhibits destabilizes β-sheet aggregates by hydrophobic and π-π stacking interaction.[37] We have recently described the mechanistic aspects of full-length Ab monomeric adsorption on a SWCNT.[35, 36, 42]

The surface, electronic and photovoltaic properties of carbon nanomaterials are increasingly being harnessed in designing sensing devices.[43] Particularly, molecular level information about the interfacial behavior of biomolecules in complex with carbon-based nanomaterials has facilitated designs of markers, sensors and actuators in diagnostic applications. Recently proposed prototypes include sensors for biomolecular conformational changes,[44] dynamics,[45] toxicity,[46,47] size,[48] sequence specificity,[49] and others.[50] Further advances could aid the development of 'point-of-care' diagnostics for evaluating metabolic and physiological conditions.[51] It has been speculated that accurate estimates of the presence

Soft Matter Accepted Manuscript

or concentration of small Aβ oligomers in biological fluids could facilitate AD diagnosis and subsequent intervention of disease progression.[52]

Motivated by the need for suitable AD diagnostics, and noting recent computational work in the proof-of-principle designs of useful biomolecular sensors,[44,46,49] we herein investigate the self-assembly and adsorption behavior of the full-length $A\beta_{1-42}$ peptide on the curved surface of a single walled carbon nanotube (SWCNT). We point out that while significant insights have been gained from studies of smaller Aβ fragments, key differences in behavior exist between segmental forms and the full length peptide.[53] Interestingly, the $A\beta_{1-42}$ form displays stronger aggregation properties and neurotoxic effects than even the $A\beta_{1-40}$ form.[54] We have earlier described the spontaneous adsorption of monomeric $A\beta_{1-42}$ on the SWCNT surface,[35,36,42] while other studies report its thermodynamic favorability to assemble into dimeric units.[55,56] Herein, we find that while the propensity of Aβ to self-associate is hindered noticeably in the presence of the SWCNT, the interactions arising from the surface are insufficient to fully dissociate the individual monomeric units. Our Adaptive Biasing Force (ABF) based free energy calculations show that while the SWCNT surface can cause a small shift in the monomer-oligomer equilibrium, the surface adsorbed states are remarkably capable of oligomeric growth. We further investigated the response of adsorbed and pure oligomeric states as functions of applied electric field strengths. Our results further demonstrate that strength of the electrical signals contain information about the oligomeric state of the adsorbed Aβ complex. However, the magnitude of the drop in signal from one oligomeric species to the next diminishes with increasing oligomer size. We discuss the implications of our observations, and how they may be leveraged for further studies aimed at designing sensors for Aβ detection in aqueous fluids.

2. Methods

Soft Matter Accepted Manuscript

General simulation protocol

All simulations were performed with the NAMD simulation package.[57] The CHARMM22 force field with the CMAP correction[58,59] was used for all the simulations. The solvent molecules were modeled with TIP3P water,[60] and requisiste counterions added to obtain charge neutral systems. The simulation box was rectangular with a minimum distance of 15 Å between any atom and a box side, three-dimensional orthorhombic periodic boundary conditions applied. Each system was first energy minimized for 10 000 steps with the conjugate gradient method. Simulations were conducted with a 2 fs timestep in the isothermal-isobaric (NPT) ensemble, unless otherwise stated. Constant temperature was maintained with Langevin dynamics at a collision frequency of 1 ps^{-1}, and a pressure of 1 atm maintained with the Nosé-Hoover method.[61,62] Electrostatic interactions were calculated with particle-mesh Ewald[63] and SHAKE[64] was used to constrain bonds involving hydrogen atoms. The cutoff for non-bonded interactions was set to 12 Å, with smoothing started from 10.5 Å.

Principle Component Analysis (PCA)

Assemblies of IDPs such as Ab are characterized by large degrees of conformational and interaction heterogeneity.[17,55,65] Cartesian Principle Component Analysis (PCA), a useful clustering technique in biomolecular simulations,[66] was used as implemented in the CARMA package[67] to identify the key conformations and interaction modes within the simulated ensembles. After removal of the translational and the rotational degrees of freedom, distributions of the first three principal components (PCs) using a root mean squared deviation (RMSD) cutoff of 2.4 Å. The ensembles were projected on to the free energy landscape of the first (PC1) and second (PC2) principle components, and representative conformations selected from the first and second most populated clusters in this landscape.

Aβ monomer

Soft Matter Accepted Manuscript

The solution state NMR structure of $A\beta_{1-42}$ peptide, obtained in a 70:30 mixture of water and hexafluoro-2-propanol, (PDB: 1Z0Q)[68] was heated at 373 K in the gas phase to generate random coil configurations. Ten of these structures were then independently simulated in expilicit water at 310 K for at least 150 ns, generating a cumulative simulation data of over 1.6 μs. The array of Aβ conformations were subjected to PCA and structures from the two most populated clusters, shown in Figures 1 a and b, were selected. The structural propensities of these conformations, presented in Figure 1 c and d, are remarkably similar to full-length Aβ conformations reported to populate the peptide's ensemble in water.[26,69] 6 ns simulations of the representative conformations were performed, and ^{15}N and $^{13}C_{\alpha}$ chemical shifts calculated with the SHIFTS program[70] were compared with corresponding experimental data.[25] Residue-wise correlation plots between the experimental and calculated chemical shifts, and values of the Pearson Correlation Coefficients (R) are presented in Figures 1 e to h.

Single-walled carbon nanotube (SWNCT)

We have considered a (6, 6) SWCNT of diameter 8.2 Å and length 99.5 Å, with the axis of the SWCNT was set parallel to the x-axis. The SWCNT coordinates were obtained with the VMD package.[71] As in previous studies,[35,36,72] the SWCNT atoms are modeled as the aromatic sp^2 carbons of the force field. To avoid possible artifacts due to edge effects, periodic boundary conditions were used to replicate the SWCNT infinitely in the x-direction. The distance from the SWCNT end to the edge of the simulation box in the x-direction was 1.5 Å.[72] The nanotube was held fixed in the setup position in all simulations with harmonic force with a force constant of 2.0 kcal mol^{-1} $Å^{-2}$.

Contact area of SWCNT-peptide complexes

Soft Matter Accepted Manuscript

As in earlier studies,[35,36,72] The contact area between the SWCNT and the peptide complexes is calculated as,

$$S = \frac{1}{2}\left[\left(SASA_{pep} + SASA_{SWCNT}\right) - SASA_{complex}\right] \quad (1)$$

Here, $SASA_{pep}$ and $SASA_{SWCNT}$ represent the solvent accessible surface area of the protein and the SWCNT, respectively, while $SASA_{complex}$ represents the solvent accessible surface of the entire complex. The solvent accessible surface area of each entity was calculated with a spherical probe of 1.8 Å diameter.

Adaptive Biasing Force (ABF) free energy calculations

Potential of mean force (PMF) calculations were carried out with the Adaptive Biasing Force (ABF) method[73,74] as implemented in the NAMD package. ABF is a thermodynamic integration method in which the mean force acting along a reaction coordinate 'σ' is used to estimate local barriers in the energy surface. The gradient of the free energy is obtained from the average force F_σ as,

$$\frac{dA(\sigma)}{d\sigma} = -\left\langle F_\sigma \right\rangle_\sigma \quad (2)$$

F_σ is accumulated over small bins within the desired range of σ. Here, the reaction coordinate used, the distance d_{in} (see *Results*), was varied from 6 to 24 Å. Three 6 Å segments were used with each segment was divided into 24 bins of 0.25 Å width, and ABF calculations carried out independently in each segment. To avoid non-equilibrium effects, unbiased sampling was carried out for 500 steps prior to application of bias. The standard deviations were obtained from the system forces using the method formulated by Rodriguez-Gomez.[75,76] The ABF simulations within each segment were carried out for 650 ns, with convergence obtained over at least 200 ns.

Soft Matter Accepted Manuscript

Application of electrical fields

1M KCl ions were randomly added to the simulation box of selected conformations of free and SWCNT surface adsorbed monomeric, dimeric and trimeric Aβ states while ensuring charge neutrality in the resultant system. This protocol is identical to the one adopted in recent simulation studies.[49] After energy minimization and 4 ns equilibration in the NPT ensemble, the systems were additionally equilibrated for 1 ns in the canonical (NVT) ensemble at 310 K. The volume of the simulation box was found to converge during the equilibration period (see Figure S1 in ESI). Following this, a uniform electric field of strength E_x was applied in the direction parallel to the SWCNT axis (ie. along the X-axis), and the system simulated under this condition for 40 ns. The corresponding potential difference is obtained as $V_x = -L_x E_x$, where E_x is the electric field applied in the x-direction, and L_x is the length of the simulation box in the x-direction. Voltages, ranging from 0.5 to 2.25 Volts, at intervals of 0.25 Volts, were applied. These are comparable to the range of voltages applied in recent computational studies.[49,46] We point out that recent studies demonstrate the compatibility of biomolecular systems with electric fields in the range of 10^8 to 10^{10} V m^{-1} (or 1.95 x 10^{-4} to 1.95 x 10^{-2} a.u, where 1 a.u 51.4 × 10^{10} Vm^{-1}).[77,78] As our simulation box size in the x-direction is ~100 Å, the strength of the external field applied along the x-direction ranged from about 9.7 x 10^{-5} to 4.4 x 10^{-4} a.u. The ionic currents resulting from application of E_x were measured as,[49,79]

$$I(t) = \frac{1}{\Delta t . L_x} \sum_{i=1}^{N} q_i . [x_i(t + \Delta t) - x_i(t)] \qquad (3)$$

Here, L_x is the system dimension in the x-direction; N is the total number of ions; q_i is the charge of the i^{th} ion; and $x_i(t)$ is the x-coordinate of the i^{th} ion at time t. Δt was chosen to be 50 ps.

Soft Matter Accepted Manuscript

3. Results and Discussion

Spontaneous small oligomeric assembly

We begin first by investigating the spontaneity of small oligomerisation in the full length Ab. As described in Methods, an ensemble of dimeric structures amounting to a cumulative simulation time of 1.5 μs was obtained from independent trajectories started by placing two monomeric units at 33 Å apart at varying relative orientations. Stable dimeric conformations were selected via principle component analysis (PCA), and the trimeric ensemble obtained by placing a third Aβ monomer at center of mass distances of 33 Å at varying orientations and generating 1.5 μs of cumulative simulation data. In Figures 2a and 2b, we depict temporal evolution of the total inter-monomer interactions for the dimer ($E_{1\text{-}2}$) and the trimer ($E_{1\text{-}2\text{-}3}$) averaged over multiple simulation trajectories. The marked strengthening of the interactions within a few tens of nanoseconds highlights the spontaneity of early oligomeric assembly of Aβ, in agreement with earlier reports.[55, 56] The mean values of $E_{1\text{-}2}$ and $E_{1\text{-}2\text{-}3}$ over the last 10 ns of the simulation trajectories are -224.6 (±65.0) and -364.1 (±72.1) kcal mol^{-1}, respectively. In Figures 2c and 2d, we describe the ensemble of conformations projected into the landscape of the first (PC1) and second (PC2) principle components, and present snapshots of the representative conformations of the first and second most populated clusters in this landscape. The representative conformations were further used for simulations of oligomer-SWCNT interactions studies described in the remainder of the paper.

SWCNT surface adsorption competes with inherent self-assembly

We have earlier described the (enthalpic) factors that lead to spontaneous adsorption of $A\beta_{1\text{-}42}$ on the outer surface of a SWCNT.[35, 36] We herein investigate whether the interactions arising from the SWCNT can compensate for the strong enthalpy driven self-assembly of the

Soft Matter Accepted Manuscript

Aβ monomer. Representative dimeric conformations (from clusters C1 and C2) were placed in the vicinity of the curved outer surface of a SWCNT of (6,6) chirality, at center of mass distances from the SWCNT varying between 15 and 20 Å. Six independent trajectories, amounting to a cumulative simulation time of 1.2 μs, were generated. Evolution of $E_{1\text{-}2}$, and that of $E_{D\text{-}NT}$, the interaction of SWCNT with the dimer complex, was monitored; these are shown for a sample trajectory in Figure 3a. The mean values of $E_{1\text{-}2}$ and $E_{D\text{-}NT}$ obtained from over last 10 ns of all trajectories were -119.1 (±41.9) and –160.3 (±32.6) kcal mol^{-1}, respectively, showing that the nanotube offsets the inter-monomer binding strength of the dimer complex by nearly 50%. For a better understanding of the interplay between the competing Aβ propensities of assembly and adsorption, we obtain probability distributions, $p(S_{D\text{-}NT}, S_D)$, of the inter-monomer (S_D) and the dimer-SWCNT ($S_{D\text{-}NT}$) contact areas from the simulated data. The contact area calculation has been described in previous studies.[35,72] The probabilities were converted to the free energy landscape (see Figure 3b) using $F(S_{D\text{-}NT}, S_D) = -k_BT \ln(p/p_{max})$, where k_B, T and p_{max} are the Boltzmann's constant, absolute temperature and the maximum probability, respectively. This landscape is presented in Figure 3b. The shallow minimum (marked 'A') corresponds to early conformations in the simulation trajectories while the deeper minima (containing 'B', 'C' and 'D') correspond to states obtained after full adsorption. The landscape is also characterized by another deep minimum (marked 'E') with a much narrower ('minor') basin. Importantly, the figure indicates that the initial states are separated from the maximally adsorbed states by a small barrier. Interestingly, the broad basin shows that the variation in S_D is markedly greater than the variation in $S_{D\text{-}NT}$. We find that that $S_{D\text{-}NT}$ is largely confined to values much lower than 1800 $Å^2$ indicating that it never exceeds twice the mean monomer-SWCNT contact area of ~900 $Å^2$.[35] The mean value of $S_{D\text{-}NT}$ is 1250.0 (±70.0) $Å^2$. Thus, while the SWCNT surface can

Soft Matter Accepted Manuscript

induce destabilization in pre-formed Aβ dimers, it cannot fully compensate for the enthalpic factors that bind the monomeric units.

We investigated the effect of the surface on the structural integrity of the dimeric complex by evaluating the 'asphericity', α, of the pure and surface adsorbed complexes. The asphericity is defined as $\alpha = 1-(I_{min}/I_{max})$, where I_{min} and I_{max}, the minimum and maximum values, respectively, of the principle moments of inertia. I_{min} and I_{max} are equal in a perfectly spherical compact object leading to $\alpha = 0$; higher α indicate a lowering of the compactness. The α distributions are compared in Figure 4a. The mean of α for the free and the surface adsorbed dimers are 0.4 (±0.2) and 1.7 (±0.9), respectively, showing that the surface reduces the overall compactness of the dimeric state, in addition to the enhanced structural fluctuation evident earlier from $S_{D\text{-}NT}$. We further evaluated the inter-monomer residue-residue contact probability map for the free and surface dimers, presented in Figure 4b. As in earlier studies,[27] a pair of residues has been considered to form a contact if the separating distance of their side-chains does not exceed 7 Å. The reduction in the total number of inter-monomer contacts due to the interaction with the surface is evident from the comparison; the average number of inter-residue contacts decreases from 34 in the free dimeric ensemble to 19 in the dimer-SWCNT ensemble, corresponding to a 44.1% reduction. The reduction in the inter-monomer contact is pronounced in the region of the central hydrophobic core, $L_{17}VFFA_{21,}$ and in the C-terminal region, $G_{29}AIIGLMVGGVVIA_{42}$ region. We have reported earlier that the hydrophobicity and the π-π interactions arising from these domains play key roles in the adsorption of Aβ on the SWCNT.[35,36]

Growth potential of oligomers immobilized on the nanosurface

Free Aβ monomers are found to be in equilibrium with small oligomeric states in aqueous medium.[22] In order to understand how binding to the nanotube may shift the monomer-

Soft Matter Accepted Manuscript

oligomer equilibrium, we compared growth potentials of a representative surface adsorbed dimeric state ('C' in the major basin of Fig 3) with that of a free dimer (from C1 of Fig 2). The ABF procedure, as described in Methods, was used to evaluate the potential of mean force (PMF) as a function of the incoming distance (d_{in}), of the center of mass of a third monomer (M_I) from a pre-adsorbed monomer of the dimeric complex. In the case of the free dimer, d_{in} was the center of mass distance between the incoming monomer and the closer, facing monomer of the dimeric complex. The resultant free energy profiles are compared in Figure 5. The most favorable approach distances in the two scenarios are close, reflected in similar positions of the free energy minimum obtained at 9.25 and 10 Å for the free and surface adsorbed complexes, respectively. However, unlike in the case of the free complex where the incoming monomer pays a small free energy cost to approach the existing dimer to within 6 Å, the corresponding penalty for the surface adsorbed complex is about three times higher. The PMF profile further shows that for the surface adsorbed complex, the thermodynamic cost for separating M_I far away from the existing complex (d_{in} ~24 Å) is about half the corresponding cost in the free complex. Thus, the free energy analysis shows that assembly and growth are possible for the surface adsorbed small Aβ complexes, but the resultant complexes are less compact and relatively more vulnerable to disassembly. This indicates that the nanotube surface is likely to cause subtle shifts in the equilibrium between the peptide's monomeric and small oligomeric states.

We have further generated multiple unbiased simulation trajectories (totaling 900 ns) started with an incoming monomer placed in the vicinity of initial dimer-SWCNT complexes selected from 'B', 'C' and 'D' of Fig 3. The mean inter-peptide (E_T) and the trimer-SWCNT ($E_{T\text{-}NT}$) interaction strengths over the last 10 ns were -222.0 (±79.6) and -271.6 (±30.0) kcal mol^{-1}, respectively, and the corresponding mean contact area of the SWCNT with the resulting trimeric complex was 1886.2 (±128.2) $Å^2$. As in dimeric adsorption, we find that

Soft Matter Accepted Manuscript

the adsorption is not proportional to the oligomeric number. Probability distribution of the inter-protein contact area (S_T) vs. the SWCNT contact area with the trimeric complex ($S_{T\text{-}NT}$) converted to a free energy landscape is provided in Figure 6; the initial 20 ns of the trajectories are not considered. Two predominant ($S_{T\text{-}NT}$, S_T) free energy basins centered at 'A', or (1700, 1700), and 'B', or (2100, 1700), are found to be in equilibrium. Thus, relative strengthening of the trimer-nanotube contacts occurs at the expense of the inter-monomer contacts, and vice-versa. Although the population centered at 'B' is slightly broader, the barrier separating the two distributions (~1 kcal mol^{-1}) can be accessed at physiological temperatures.

Electrical responses can distinguish adsorbed small oligomeric states of Aβ

Recent MD reports show that ionic currents obtained upon the application of suitable electric fields to biomolecular complexes with carbon nanomaterials can yield useful molecular information such as the sequence specificity of DNA basepairs,[49] protein nanotoxicity[46] and others.[48,80] We herein examined whether appropriate electrical responses of the adsorbed states could be useful in detecting the size of adsorbed small oligomeric species of Aβ. As described in *Methods*, representative free and surface adsorbed monomeric, dimeric and trimeric conformations, as well as an isolated SWCNT were inserted into a simulation box containing ionic solution and subjected to varying electrostatic potential differences. In Figures 7a and b, respectively, we present the ionic currents obtained for the free (I_M; I_D; I_T) and surface adsorbed ($I_{M\text{-}NT}$; $I_{D\text{-}NT}$; $I_{T\text{-}NT}$) monomeric, dimeric and trimeric states at a potential difference of 0.5 Volts; the ionic current obtained for the isolated SWCNT (I_{NT}) is also shown in Figure 7 b. Corresponding data obtained at 1.25 Volts are shown in Figures 7c and 7d, respectively; at 1.75 Volts in Figures 7e and 7f, respectively; and at 2.25 Volts in Figure 7g and 7h, respectively. We note here that the currents associated with each system for a

Soft Matter Accepted Manuscript

constant E_x are characterized by significant fluctuations that appear to increase slightly with the strength of the applied field. In Table 2, we have provided mean values of the ionic currents, along with their standard deviations, for the isolated SWCNT, and the free and surface adsorbed monomeric, dimeric and trimeric states at all applied potential differences.

At a potential difference of 0.5 Volts, the currents of the individual systems are almost indistinguishable, although the mean value of I_{NT} is about 4 nA higher than the mean value of $I_{T\text{-}NT}$. These differences grow with increasing voltages, and at a potential difference of 1.25 Volts, the currents of the adsorbed states can be clearly distinguished from each other and from I_{NT}. As seen from the tabulated data, for a fixed applied potential difference, the current obtained for a given adsorbed state is comparable to the current obtained for the corresponding free state. It is noteworthy that the current difference between the free and the adsorbed states are more pronounced for the monomeric states than for the oligomeric states. The drops in the ionic current of the adsorbed state over the current in the free state span 3.5% to 13.7%, as calculated from the values of I_M and $I_{M\text{-}NT}$ at the lowest and the highest applied potential differences.

We note an additional interesting characteristic of current responses of the simulated systems. For every applied potential difference, the magnitude of the drop in $I_{M\text{-}NT}$ over I_{NT} is greater than the magnitude of the drop in $I_{D\text{-}NT}$ over $I_{M\text{-}NT}$, which in turn is greater than the magnitude of the drop in $I_{T\text{-}NT}$ over $I_{D\text{-}NT}$. Thus, the ionic current blockades are not simply proportional to the size of the adsorbed aggregate, but have a complex dependence on the adsorbed state. This phenomenon is visualized clearly in Figure 8, where we have plotted values of the mean ionic currents for each system as functions of the applied voltage. It is evident from these analyses, however, that at sufficiently high (beyond 1.25 Volts) potential differences, the drop in ionic current of an adsorbed Aβ complex relative to the ionic current signal in the isolated SWCNT is informative of the number of monomers in the complex.

Soft Matter Accepted Manuscript

Further investigations will be necessary to reveal the nature of fluctuations within the ionic currents, the size of the adsorbed aggregate at which the ionic currents may be rendered indistinguishable, and the microscopic origins of the reduction in current blockades with increasing oligomeric size.

Applied fields cause minor perturbation within the adsorbed states

In the light of the above possibilities, it is important to evaluate the extent to which the applied electric fields induce desorption of the Aβ complexes from the nanosurface, or induce oligomeric dissociation. To this end, we first compared the degrees of immobilization of the surface adsorbed oligomers in the absence and presence of the electric field. The mean squared distances ($<\Delta r^2>$, or MSD) as a function of time were calculated for the centers of mass of the monomers, dimers and trimers in each case and compared with the corresponding MSD of the free states. This comparison (with the MSD plots corresponding to the highest applied voltage of 2.25 Volts) is presented in Figure 9. The MSD plots are almost linear for the free states, indicating their unrestricted, largely diffusive behavior in pure solvent environment. Further, as expected, there is a lowering in the slope of the MSD plot with increase in oligomeric size. The diffusions coefficients (D) for the free monomer, dimer and trimeric states, obtained from linear fits of the MSD and Stokes-Einstein's relationship, were 1.1×10^{-6}, 0.63×10^{-6} and 0.35×10^{-6} cm^2 sec^{-1}, respectively. We note that D calculated for the free monomeric and dimeric state in this study are identical to those reported elsewhere.[55] Surface adsorption on the SWCNT surface imposes marked restrictions on the translational diffusion for the monomeric and the oligomeric states, as is evident from the sharp lowering of the slope of the MSD curve and greater deviations from linear behavior at high t. Upon application of the electric field, the MSD slope is increased to some extent but is still markedly lower compared to the free states. The electric field, however, induces greater non-

Soft Matter Accepted Manuscript

linearity in the MSD at high *t*, indicating a greater deviation from diffusive behavior in the presence of the field. Interestingly, upon evaluation of the rotational time correlation function, $<\boldsymbol{R}(0)\cdot\boldsymbol{R}(t)>$, of the unit vector $\boldsymbol{R}(t)$ connecting the first and the last C_α atoms of each Aβ unit, we found a significant slowdown of their overall rotational dynamics upon surface adsorption. A marginal enhancement in the rotational dynamics was observed upon application of the electric fields (see Figure S2 in ESI).

Comparison of the MSD at the highest applied field strength with the free states indicates that the strongest applied field, while enhancing the mobilities of the adsorbed monomer and oligomers, does not cause oligomeric desorption from the surface and their release into the solution. For verification, we compared comparing the inter-peptide and peptide-nanotube interaction strengths along with the peptide-nantoube contact area in the absence and in the presence of the electric fields. This comparison, with data obtained at 0.0 (ie. absence of applied electric field), 0.75 and 2.25 Volts, is presented in Table 3. The decrease in magnitudes of the mean values $E_{1\text{-}2}$ and $E_{1\text{-}2\text{-}3}$ even at 2.25 Volts over corresponding values at 0.0 Volts is found to be negligible. The decrease in the strength of $E_{M\text{-}NT}$, $E_{D\text{-}NT}$ and $E_{T\text{-}NT}$ are relatively more noticeable, being 16.2% 6.2% and 6.7% less, respectively, than the values at 0.0 Volts. The mean contact area of the peptide complexes with the SWCNT also change very marginally; the decrease in $S_{M\text{-}NT}$, $S_{D\text{-}NT}$ and $S_{T\text{-}NT}$ at 2.25 Volts over corresponding values at 0.0 Volts are 5.4%, 3.6% and 2.7% respectively. This analysis corroborates the earlier observation that the applied electric fields are not sufficient to induce major instabilities in the adsorbed states. We do not expect, therefore, the monomer-oligomer equilibrium to change markedly in the presence of the strongest electric field applied in this study.

Summary and Conclusion

Soft Matter Accepted Manuscript

In summary, this work establishes the competitive nature of Aβ self-assembly and its adsorption propensity on the SWCNT nanosurface, and demonstrates the detectability of adsorbed oligomeric states through differential ionic currents upon application of optimal electric fields. Although Aβ dimers have a marked weakening upon surface adsorption on the SWCNT, they are capable of growing into trimeric assemblies. Free energy calculations demonstrate that only a small shift in the dimer-trimer equilibrium in solution should occur in the surface adsorbed states over the free oligomeric states. The results provide a basis for the development of carbon nanomaterial based prototypical electrical sensors aimed at detecting the presence of Aβ monomers and small oligomers in aqueous media, and possibly in biological fluids.

Continuing studies in our laboratory will investigate microscopic origins of the fluctuations induced by the SWCNT and the origin of the non-diffusive behavior induced by the application of the electric fields. It is noteworthy that suitably functionalized CNTs offer a number of advantages, such as increased solubility and chemical functionality over pristine CNTs.[81, 82] We will therefore seek to understand how suitable physico-chemical alterations to the SWCNT characteristics may influence the electrical responses, and strategies to leverage those findings in the design of optimal sensors for small Aβ oligomers, as well as its higher ordered assemblies. We further point out that replacing armchair SWCNTs with conducting nanotubes[83] could enable the use of electrical signals generated within the device itself. Precise experiments and advanced computational methods[84] could be used to study surface charge transport in functionalized SWCNTs under suitable fields, to design devices for detecting the state of Aβ assemblies.

Before concluding, we remark that Aβ is just one member of a family of IDPs whose small oligomers and amyloid assemblies are associated with a debilitating disease.[6] Different IDPs exhibit marked differences in self-assembly kinetics and are likely to trigger diseases

Soft Matter Accepted Manuscript

onset at different stages during the assembly pathway. Interestingly, emerging research indicate overlapping etiologies for several of neurodegenerative proteopathies arising from co-assembly of IDPs associated with individual disorders.[85, 86] It may therefore be worthwhile to investigate how other IDPs aggregate and adsorb on surfaces, the equilibrium of the adsorbed states with the monomers present in aqueous solution, and whether these states can be detected via their unique responses to electrical stimulation.

Acknowledgments

Funding for this project was received from the CSIR 12th Five Year Plan 'Multi-Scale Simulation and Modeling' project (MSM; grant number CSC0129). Additional resources from the Center of Excellence in Polymers (CoEP-SPIRIT), established from funding received from the Department of Chemicals and Petrochemicals is acknowledged. A.K.J thanks University Grants Commision (UGC) for his Senior Research Fellowship. We thank Professor M. G. Zagorski for providing the chemical shift values for Aβ. A.K.J thanks Mr. Turbasu Sengupta for help with graphics, Ms. Jaya C. Jose for help with chemical shift calculations, and Dr. Srinivasa Murthy Gopal and Mr. Xavier Prasanna for discussions.

Figures

Soft Matter Accepted Manuscript

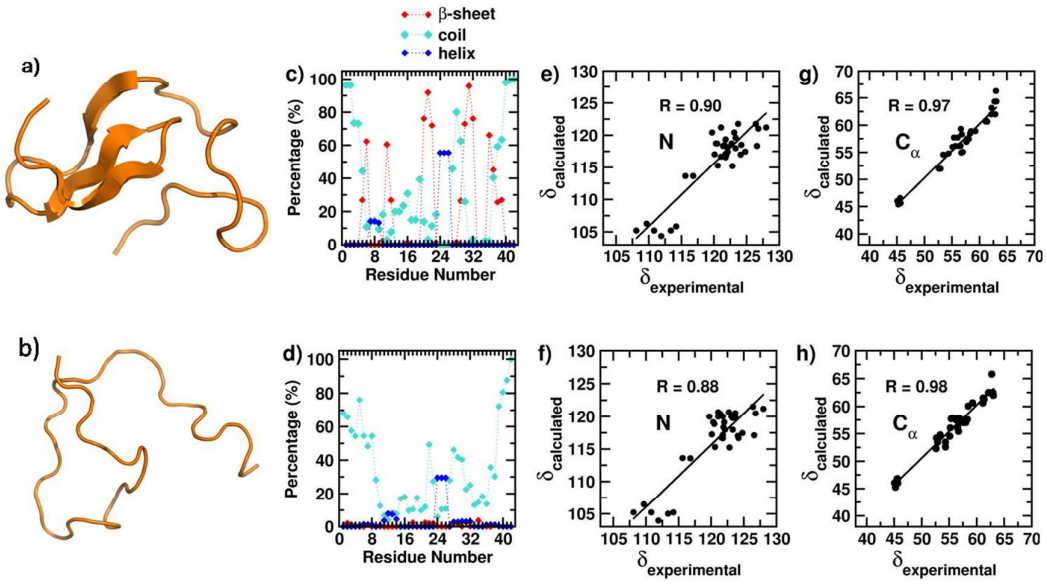

Figure 1. a), b) Snapshots of representative monomer conformations used in this study ; c), d) corresponding residue-wise secondary structure propensity. For the conformation in a), correlation of the average ^{15}N and $^{13}C_\alpha$ NMR chemical shifts with corresponding experimental values are shown in e) and g); the data for the conformation in b) are shown in f) and h). Linear regressions of the calculated ($\delta_{calculated}$) and the experimental ($\delta_{experimental}$) chemical shifts are provided with the Pearson Correlation Coefficients (R).

Soft Matter Accepted Manuscript

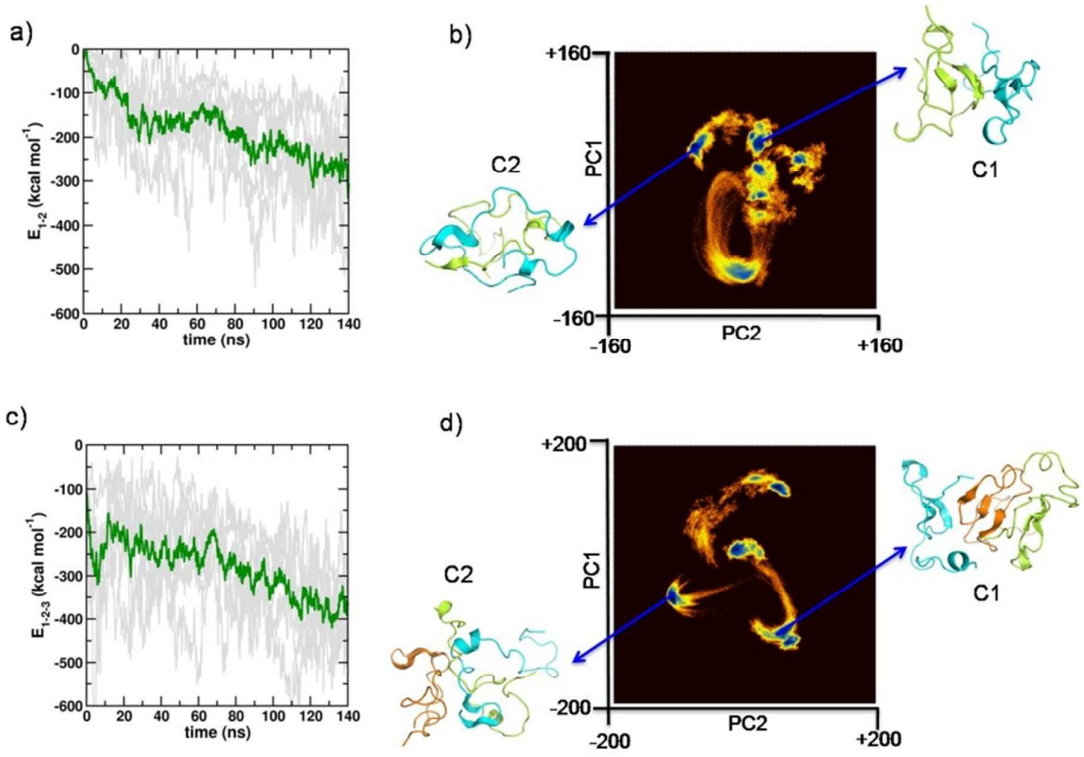

Figure 2. Time evolution of the total inter-monomer interaction energies in a) dimerizing simulations ($E_{1\text{-}2}$) and c) trimerizing simulations ($E_{1\text{-}2\text{-}3}$). Evolutions over individual trajectories are depicted in gray, and the mean over multiple trajectories in *green*. Free energy landscape as a function of the first (PC1) and second (PC2) principal components for the b) dimer ensemble, and d) the trimer ensemble. Representative snapshots of the first and the second most populated clusters are depicted as C1 and C2, respectively.

Soft Matter Accepted Manuscript

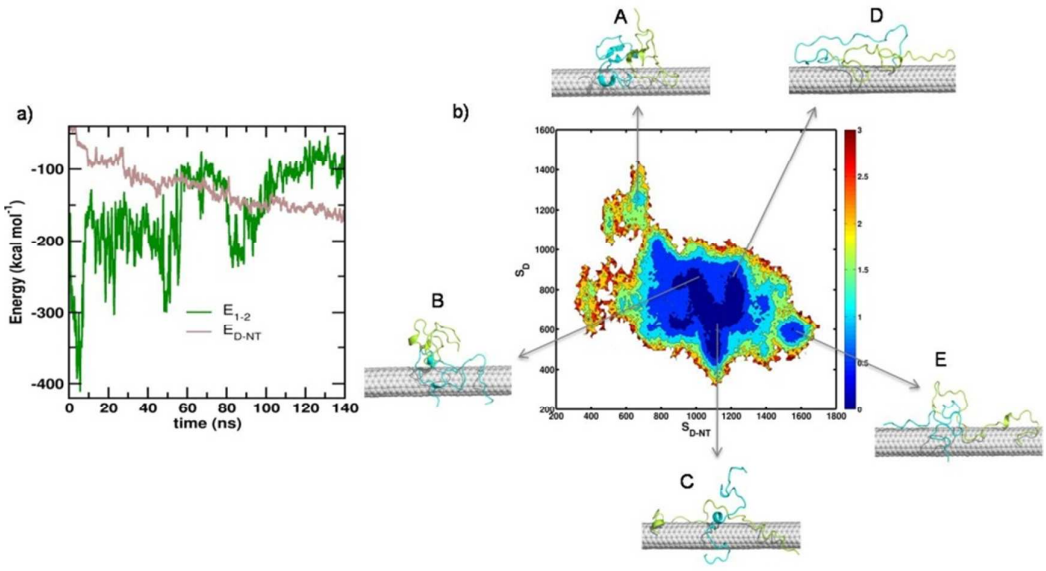

Figure 3. a) Time evolution of $E_{1\text{-}2}$ and $E_{D\text{-}NT}$ (see main text), from a representative simulation of surface bound dimeric system; b) Free energy landscape as function of inter-protein contact area (S_D, in $Å^2$) and nanotube-protein contact area ($S_{D\text{-}NT}$, in $Å^2$) for surface bound dimeric complexes. Representative snapshots in the free energy landscape are depicted are labeled as 'A', 'B', 'C', 'D' and 'E' (see main text). Units of free energy kcal mol^{-1}.

Soft Matter Accepted Manuscript

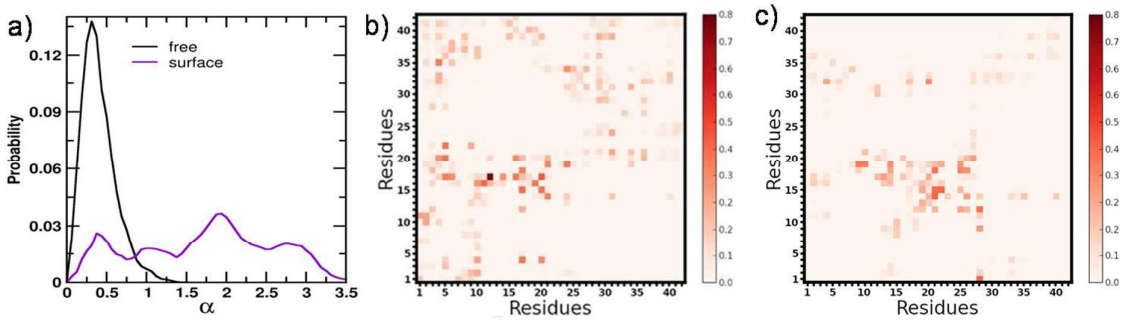

Figure 4. a) Probability distributions of the asphericity α for free and surface bound dimers. Inter-monomer residue-wise contact probabilities for the b) free, c) surface bound dimeric ensembles.

Soft Matter Accepted Manuscript

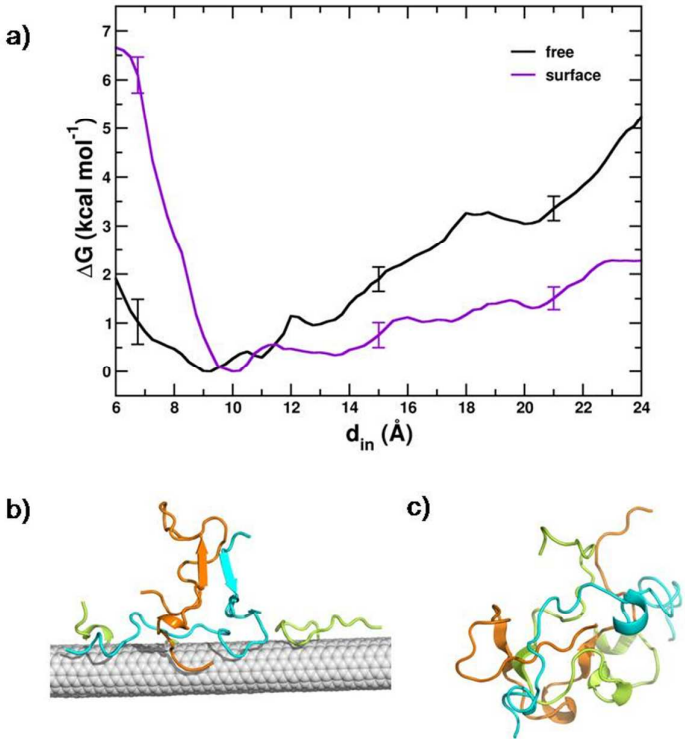

Figure 5. a) ABF based free energy profiles as a function of distance (d_{in}) of an incoming third monomer to a pre-existing free and surface adsorbed dimeric complex. Snapshots corresponding to the free energy minimum are shown for b) surface adsorbed, and c) free complexes.

Soft Matter Accepted Manuscript

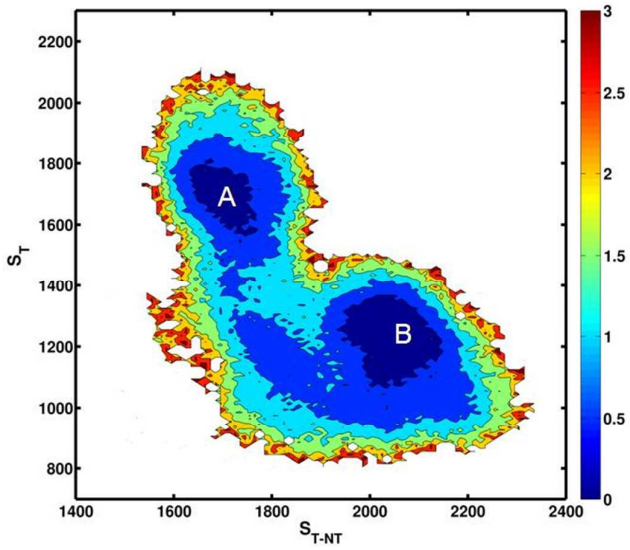

Figure 6. Free energy landscape as function of inter-protein contact area (S_T, in $Å^2$) and nanotube-protein contact area ($S_{T\text{-}NT}$, in $Å^2$) for surface bound trimeric complexes. Units for free energy are kcal mol^{-1}.

Soft Matter Accepted Manuscript

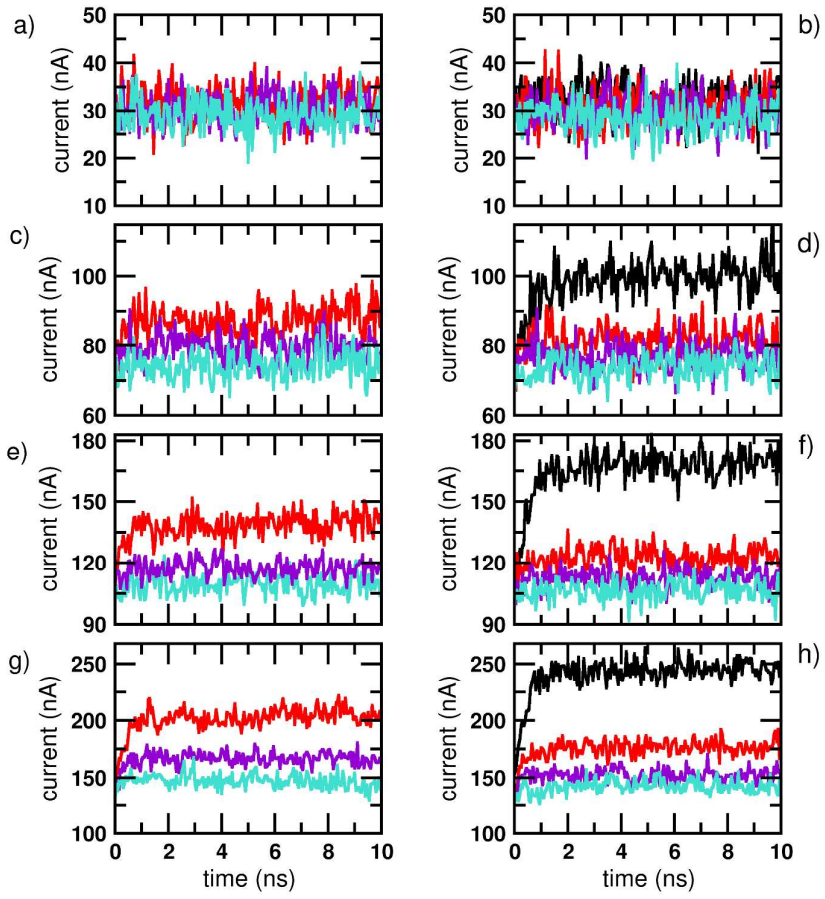

Figure 7. Ionic currents (in nA) as a function of simulation time for sample trajectories of the free and adsorbed monomeric (in red), dimeric (in purple) and trimeric (in cyan) states, and in the isolated SWCNT (in black). The applied potential differences are in a) and b) 0.5 Volts; in c) and d) 1.25 Volts; in e) and f) 1.75 Volts; in g) and h) 2.25 Volts. The currents for the free states (I_M, I_D, I_T) are in a), c), e) and g); the currents for the isolated SWCNT (I_{NT}) and the adsorbed states ($I_{M\text{-}NT}$, $I_{D\text{-}NT}$, $I_{T\text{-}NT}$) are in b), d), f) and h).

Soft Matter Accepted Manuscript

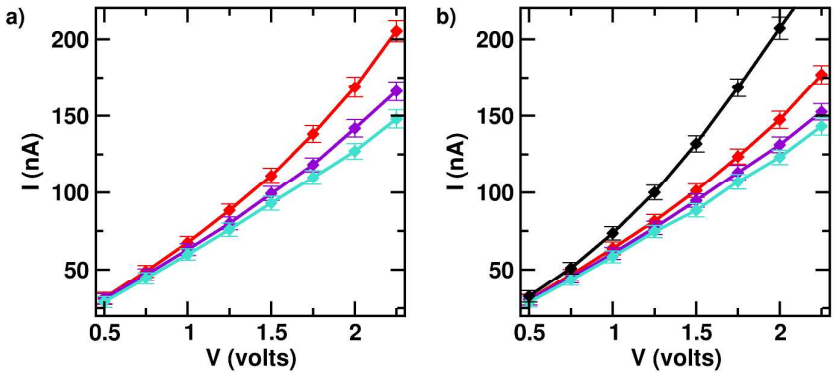

Figure 8. Mean ionic current as a function of applied voltage for a) free and b) surface adsorbed monomeric (red), dimeric (purple) and trimeric (cyan) complexes. The mean ionic current for the isolated SWCNT (black) is provided in b).

Soft Matter Accepted Manuscript

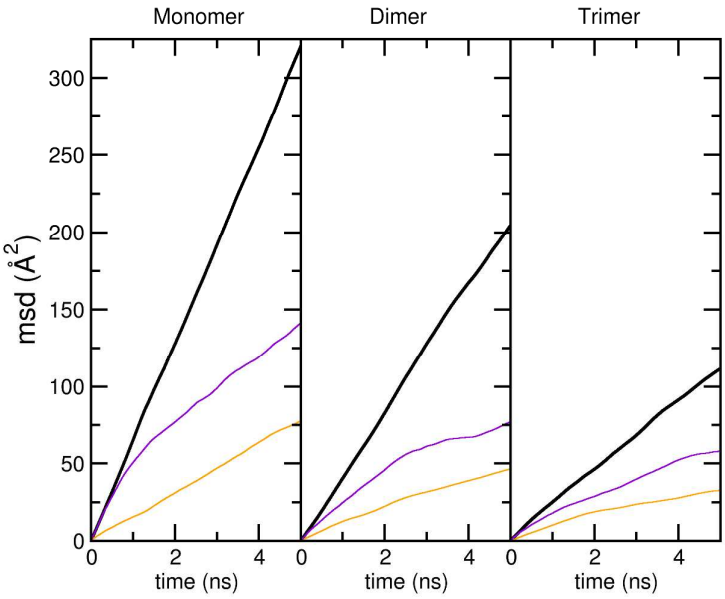

Figure 9. Mean squared displacement (msd) of the center of masses of the monomer, dimer and trimer complexes in the free state (in black), upon surface adsorption on the SWCNT (in orange) and upon the application of the electric field corresponding to a potential difference of 2.25 Volts (in purple).

Soft Matter Accepted Manuscript

Tables

PD	0.5	0.75	1.0	1.25	1.50	1.75	2.0	2.25
$E_x \times 10^{-3}$ (V Å^{-1})	5.01	7.51	10.02	12.52	15.03	17.53	20.04	22.54
$E_x \times 10^{-4}$ (in a.u)	0.97	1.46	1.95	2.43	2.92	3.41	3.90	4.40

Table 1. The potential differences (PD, in Volts) used in this study, and the corresponding electric fields (E_x) applied parallel to the SWCNT axis, in Volts Å^{-1} and in atomic units (a.u).

Soft Matter Accepted Manuscript

PD	0.5	0.75	1.0	1.25	1.5	1.75	2.0	2.25
I_{NT}	32.6	51.1	73.6	99.9	131.8	168.6	207.0	244.4
	(3.6)	(3.8)	(4.3)	(4.8)	(5.2)	(5.9)	(7.0)	(7.5)
I_{M}	31.5	49.0	67.6	88.3	110.9	138.2	168.8	205.1
	(3.7)	(3.9)	(3.9)	(4.2)	(5.1)	(5.5)	(6.6)	(6.7)
I_{M-NT}	30.4	46.7	63.9	81.4	101.0	123.5	147.5	177.0
	(3.5)	(3.6)	(4.1)	(4.1)	(4.4)	(4.9)	(5.6)	(5.9)
I_{D}	30.8	46.8	63.1	80.0	99.2	118.1	141.8	166.2
	(3.5)	(3.8)	(3.8)	(4.1)	(4.6)	(4.6)	(5.7)	(6.3)
I_{D-NT}	30.2	44.9	60.6	77.1	94.6	113.0	131.1	152.6
	(3.4)	(3.7)	(3.9)	(4.2)	(4.3)	(4.7)	(5.1)	(5.3)
I_{T}	28.9	44.4	60.0	76.0	93.0	109.8	126.9	148.0
	(3.5)	(3.8)	(3.6)	(4.3)	(4.4)	(4.6)	(5.2)	(6.0)
I_{T-NT}	28.8	43.5	58.5	74.7	88.4	106.9	123.1	143.2
	(3.3)	(3.6)	(3.8)	(3.9)	(4.2)	(4.9)	(4.7)	(5.6)

Table 2. The mean ionic currents (in nanoAmperes) obtained at the range of potential differences (PD, in Volts), for the isolated SWCNT (I_{NT}); the pure (I_M) and the surface adsorbed (I_{M-NT}) monomeric states; the pure (I_D) and the surface adsorbed (I_{D-NT}) dimeric states; and the pure (I_T) and the surface adsorbed (I_{T-NT}) trimeric states. Standard deviations are provided in braces.

Soft Matter Accepted Manuscript

PD	$E_{1\text{-}2}$	$E_{1\text{-}2\text{-}3}$	$E_{M\text{-}NT}$	$E_{D\text{-}NT}$	$E_{T\text{-}NT}$	$S_{M\text{-}NT}$	$S_{D\text{-}NT}$	$S_{T\text{-}NT}$
0.0	-119.1	-222.0	-128.8	-160.3	-271.6	935.6	1250.0	1886.2
	(41.9)	(79.6)	(11.2)	(32.6)	(30.0)	(52.7)	(70.0)	(128.2)
0.75	-117.9	-217.9	-108.4	-149.9	-256.4	892.3	1205.0	1840.4
	(38.5)	(70.0)	(18.8)	(35.3)	(32.2)	(47.9)	(70.9)	(128.8)
2.25	-117.0	-218.5	-107.9	-150.3	-253.3	885.0	1205.4	1835.2
	(40.0)	(70.5)	(20.0)	(36.0)	(38.8)	(49.0)	(72.0)	(130.0)

Table 3. The mean inter-protein interaction strengths in the adsorbed dimeric ($E_{1\text{-}2}$) and adsorbed trimeric ($E_{1\text{-}2\text{-}3}$) states; the mean monomer-surface ($E_{M\text{-}NT}$), the dimer-surface ($E_{D\text{-}NT}$) and the trimer-surface ($E_{T\text{-}NT}$) interactions; and the mean monomer-surface ($S_{M\text{-}NT}$), the dimer-surface ($S_{D\text{-}NT}$) and the trimer-surface ($S_{T\text{-}NT}$) contact areas. The data are provided at applied potential difference (PD) of 0.0 Volts (no applied electric field), 0.75 Volts, and 2.25 Volts. The units of interaction strength and contact area are kcal mol^{-1} and $Å^2$, respectively. Standard deviations are provided in braces.

Electronic Supplementary Information (ESI) available.

Soft Matter Accepted Manuscript

References

1. M. Mahmoudi, H. R. Kalhor, S. Laurent and I. Lynch, *Nanoscale*, 2013, 5, 2570-2588.
2. C. Li and R. Mezzenga, *Nanoscale*, 2013, 5, 6207-6218.
3. Y. D. Álvarez, J. A. Fauerbach, J. s. V. Pellegrotti, T. M. Jovin, E. A. Jares-Erijman and F. D. Stefani, *Nano Letters*, 2013, 13, 6156-6163.
4. P. Tompa, *Trends in Biochemical Sciences*, 2012, 37, 509-516.
5. F. U. Hartl, A. Bracher and M. Hayer-Hartl, *Nature*, 2011, 475, 324-332.
6. F. Chiti and C. M. Dobson, *Annual Review of Biochemistry*, 2006, 75, 333-366.
7. S. L. Bernstein, T. Wyttenbach, A. Baumketner, J.-E. Shea, G. Bitan, D. B. Teplow and M. T. Bowers, *Journal of the American Chemical Society*, 2005, 127, 2075-2084.
8. S. Gnanakaran, R. Nussinov and A. E. Garcia, *Journal of the American Chemical Society*, 2006, 128, 2158-2159.
9. R. Pellarin, E. Guarnera and A. Caflisch, *Journal of Molecular Biology*, 2007, 374, 917-924.
10. M. G. Krone, L. Hua, P. Soto, R. Zhou, B. J. Berne and J.-E. Shea, *Journal of the American Chemical Society*, 2008, 130, 11066-11072.
11. Y. Miller, B. Ma and R. Nussinov, *Proceedings of the National Academy of Sciences of the United States of America*, 2010, 107, 9490-9495.
12. R. Krishnan, J. L. Goodman, S. Mukhopadhyay, C. D. Pacheco, E. A. Lemke, A. A. Deniz and S. Lindquist, *Proceedings of the National Academy of Sciences of the United States of America*, 2012, 109, 11172-11177.
13. D. Thirumalai, G. Reddy and J. E. Straub, *Accounts of Chemical Research*, 2012, 45, 83-92.
14. M. Varshney, P. S. Waggoner, C. P. Tan, K. Aubin, R. A. Montagna and H. G. Craighead, *Analytical Chemistry*, 2008, 80, 2141-2148.
15. C. Cabaleiro-Lago, I. Lynch, K. A. Dawson and S. Linse, *Langmuir*, 2009, 26, 3453-3461.
16. J. A. Yang, W. Lin, W. S. Woods, J. M. George and C. J. Murphy, *The Journal of Physical Chemistry B*, 2014, 118, 3559-3571.
17. Y. Miller, B. Ma and R. Nussinov, *Chemical Reviews*, 2010, 110, 4820-4838.
18. M. M. Pallitto and R. M. Murphy, *Biophysical Journal*, 2001, 81, 1805-1822.
19. J. E. Straub and D. Thirumalai, *Annual Review of Physical Chemistry*, 2011, 62, 437-463.

Soft Matter Accepted Manuscript

20. C. Haass and D. J. Selkoe, *Nature Reviews Molecular Cell Biology*, 2007, 8, 101-112.
21. S. L. Bernstein, N. F. Dupuis, N. D. Lazo, T. Wyttenbach, M. M. Condron, G. Bitan, D. B. Teplow, J.-E. Shea, B. T. Ruotolo, C. V. Robinson and M. T. Bowers, *Nature Chemistry*, 2009, 1, 326-331.
22. S. Nag, B. Sarkar, A. Bandyopadhyay, B. Sahoo, V. K. A. Sreenivasan, M. Kombrabail, C. Muralidharan and S. Maiti, *Journal of Biological Chemistry*, 2011, 286, 13827-13833.
23. G. Bitan, M. D. Kirkitadze, A. Lomakin, S. S. Vollers, G. B. Benedek and D. B. Teplow, *Proceedings of the National Academy of Sciences of the United States of America*, 2003, 100, 330-335.
24. J. T. Jarrett, E. P. Berger and P. T. Lansbury, *Biochemistry*, 1993, 32, 4693-4697.
25. L. Hou, H. Shao, Y. Zhang, H. Li, N. K. Menon, E. B. Neuhaus, J. M. Brewer, I.-J. L. Byeon, D. G. Ray, M. P. Vitek, T. Iwashita, R. A. Makula, A. B. Przybyla and M. G. Zagorski, *Journal of the American Chemical Society*, 2004, 126, 1992-2005.
26. N. G. Sgourakis, Y. Yan, S. A. McCallum, C. Wang and A. E. Garcia, *Journal of Molecular Biology*, 2007, 368, 1448-1457.
27. C. Lee and S. Ham, *Journal of Computational Chemistry*, 2010, 32, 349-355.
28. T. Luhrs, C. Ritter, M. Adrian, D. Riek-Loher, B. Bohrmann, H. Dobeli, D. Schubert and R. Riek, *Proceedings of the National Academy of Sciences of the United States of America*, 2005, 102, 17342-17347.
29. J. Khandogin and C. L. Brooks, *Proceedings of the National Academy of Sciences of the United States of America*, 2007, 104, 16880-16885.
30. F. Massi and J. E. Straub, *Proteins: Structure, Function, and Bioinformatics*, 2001, 42, 217-229.
31. C. Cabaleiro-Lago, F. Quinlan-Pluck, I. Lynch, K. A. Dawson and S. Linse, *ACS Chemical Neuroscience*, 2010, 1, 279-287.
32. D. Brambilla, R. Verpillot, B. Le Droumaguet, J. Nicolas, M. Taverna, J. Kona, B. Lettiero, S. H. Hashemi, L. De Kimpe, M. Canovi, M. Gobbi, V. r. Nicolas, W. Scheper, S. M. Moghimi, I. Tvaroska, P. Couvreur and K. Andrieux, *ACS Nano*, 2012, 6, 5897-5908.
33. Q. Ma, G. Wei and X. Yang, *Nanoscale*, 2013, 5, 10397-10403.
34. W.-h. Wu, X. Sun, Y.-p. Yu, J. Hu, L. Zhao, Q. Liu, Y.-f. Zhao and Y.-m. Li, *Biochemical and Biophysical Research Communications*, 2008, 373, 315-318.
35. A. K. Jana and N. Sengupta, *Biophysical Journal*, 2012, 102, 1889-1896.

Soft Matter Accepted Manuscript

36. A. K. Jana, J. C. Jose and N. Sengupta, *Physical Chemistry Chemical Physics*, 2013, 15, 837-844.
37. H. Li, Y. Luo, P. Derreumaux and G. Wei, *Biophysical Journal*, 2011, 101, 2267-2276.
38. S. A. Andujar, F. Lugli, S. Hofinger, R. D. Enriz and F. Zerbetto, *Physical Chemistry Chemical Physics*, 2012, 14, 8599-8607.
39. Q. Li, L. Liu, S. Zhang, M. Xu, X. Wang, C. Wang, F. Besenbacher and M. Dong, *Chemistry – A European Journal*, 2014, 20, 7236-7240.
40. J. E. Kim and M. Lee, *Biochemical and Biophysical Research Communications*, 2003, 303, 576-579.
41. M. Mahmoudi, O. Akhavan, M. Ghavami, F. Rezaee and S. M. A. Ghiasi, *Nanoscale*, 2012, 4, 7322-7325.
42. A. K. Jana and N. Sengupta, *Biophysical Chemistry*, 2013, 184, 108-115.
43. D. Jariwala, V. K. Sangwan, L. J. Lauhon, T. J. Marks and M. C. Hersam, *Chemical Society Reviews*, 2013, 42, 2824-2860.
44. R. R. Johnson, B. J. Rego, A. T. C. Johnson and M. L. Klein, *The Journal of Physical Chemistry B*, 2009, 113, 11589-11593.
45. Y. Choi, I. S. Moody, P. C. Sims, S. R. Hunt, B. L. Corso, I. Perez, G. A. Weiss and P. G. Collins, *Science*, 2012, 335, 319-324.
46. B. Luan and R. Zhou, *The Journal of Physical Chemistry Letters*, 2012, 3, 2337-2341.
47. C. A. Jimenez-Cruz, S.-g. Kang and R. Zhou, *Wiley Interdisciplinary Reviews: Systems Biology and Medicine*, 2014, 6, 265-279.
48. K. J. Freedman, C. W. Ahn and M. J. Kim, *ACS Nano*, 2013, 7, 5008-5016.
49. C. Sathe, X. Zou, J.-P. Leburton and K. Schulten, *ACS Nano*, 2011, 5, 8842-8851.
50. M. Ferrari, *Nature Reviews Cancer*, 2005, 5, 161-171.
51. D. A. Giljohann and C. A. Mirkin, *Nature*, 2009, 462, 461-464.
52. R. J. Perrin, A. M. Fagan and D. M. Holtzman, *Nature*, 2009, 461, 916-922.
53. A. E. Conicella and N. L. Fawzi, *Biochemistry*, 2014, 53, 3095-3105.
54. M. Q. Liao, Y. J. Tzeng, L. Y. X. Chang, H. B. Huang, T. H. Lin, C. L. Chyan and Y. C. Chen, *FEBS Letters*, 2007, 581, 1161-1165.
55. X. Zhu, R. P. Bora, A. Barman, R. Singh and R. Prabhakar, *The Journal of Physical Chemistry B*, 2012, 116, 4405-4416.
56. S.-H. Chong and S. Ham, *Proceedings of the National Academy of Sciences of the United States of America*, 2012, 109, 7636-7641.

Soft Matter Accepted Manuscript

57. L. Kale, R. Skeel, M. Bhandarkar, R. Brunner, A. Gursoy, N. Krawetz, J. Phillips, A. Shinozaki, K. Varadarajan and K. Schulten, *Journal of Computational Physics*, 1999, 151, 283-312.

58. A. D. MacKerell, D. Bashford, Bellott, R. L. Dunbrack, J. D. Evanseck, M. J. Field, S. Fischer, J. Gao, H. Guo, S. Ha, D. Joseph-McCarthy, L. Kuchnir, K. Kuczera, F. T. K. Lau, C. Mattos, S. Michnick, T. Ngo, D. T. Nguyen, B. Prodhom, W. E. Reiher, B. Roux, M. Schlenkrich, J. C. Smith, R. Stote, J. Straub, M. Watanabe, J. Wiórkiewicz-kuczera, D. Yin and M. Karplus, *J. Phys. Chem. B.*, 1998, 102, 3586-3616.

59. A. D. Mackerell, M. Feig and C. L. Brooks, *J. Comput. Chem.*, 2004, 25, 1400-1415.

60. W. L. Jorgensen, J. Chandrasekhar, J. D. Madura, R. W. Impey and M. L. Klein, *The Journal of Chemical Physics*, 1983, 79, 926-935.

61. G. J. Martyna, D. J. Tobias and M. L. Klein, *The Journal of Chemical Physics*, 1994, 101, 4177-4189.

62. S. E. Feller, Y. Zhang, R. W. Pastor and B. R. Brooks, *The Journal of Chemical Physics*, 1995, 103, 4613-4621.

63. U. Essmann, L. Perera, M. L. Berkowitz, T. Darden, H. Lee and L. G. Pedersen, *The Journal of Chemical Physics*, 1995, 103, 8577-8593.

64. J.-P. Ryckaert, G. Ciccotti and H. J. C. Berendsen, *Journal of Computational Physics*, 1977, 23, 327-341.

65. G. Wei, A. I. Jewett and J.-E. Shea, *Physical Chemistry Chemical Physics*, 2010, 12, 3622-3629.

66. K. Tai, T. Shen, U. Börjesson, M. Philippopoulos and J. A. McCammon, *Biophysical Journal*, 2001, 81, 715-724.

67. N. M. Glykos, *Journal of Computational Chemistry*, 2006, 27, 1765-1768.

68. T. Simona, E. Veronica, V. Paolo, A. J. v. N. Nico, M. J. J. B. Alexandre, G. Remo, T. Teodorico, A. T. Piero and P. Delia, *ChemBioChem*, 2006, 7, 257-267.

69. Y.-S. Lin, G. R. Bowman, K. A. Beauchamp and V. S. Pande, *Biophysical Journal*, 2012, 102, 315-324.

70. K. Osapay and D. A. Case, *Journal of the American Chemical Society*, 1991, 113, 9436-9444.

71. W. Humphrey, A. Dalke and K. Schulten, *J. Mol. Graph.*, 1996, 14, 33-38.

72. C.-c. Chiu, G. R. Dieckmann and S. O. Nielsen, *The Journal of Physical Chemistry B*, 2008, 112, 16326-16333.

Soft Matter Accepted Manuscript

73. E. Darve, D. Rodriguez-Gomez and A. Pohorille, *The Journal of Chemical Physics*, 2008, 128, 144120-144113.
74. J. Hénin, G. Fiorin, C. Chipot and M. L. Klein, *Journal of Chemical Theory and Computation*, 2009, 6, 35-47.
75. D. Rodriguez-Gomez, E. Darve and A. Pohorille, *The Journal of Chemical Physics*, 2004, 120, 3563-3578.
76. J. Henin and C. Chipot, *The Journal of Chemical Physics*, 2004, 121, 2904-2914.
77. A. A. Arabi and C. F. Matta, *Physical Chemistry Chemical Physics*, 2011, 13, 13738-13748.
78. B. J. Dutta and P. K. Bhattacharyya, *The Journal of Physical Chemistry B*, 2014, DOI: 10.1021/jp5047535.
79. A. Aksimentiev, J. B. Heng, G. Timp and K. Schulten, *Biophysical Journal*, 2004, 87, 2086-2097.
80. Z. He, J. Zhou, X. Lu and B. Corry, *ACS Nano*, 2013, 7, 10148-10157.
81. C. A. Dyke and J. M. Tour, *Chemistry – A European Journal*, 2004, 10, 812-817.
82. Y. Liu, C. Chipot, X. Shao and W. Cai, *The Journal of Physical Chemistry C*, 2011, 115, 1851-1856.
83. M. F. L. De Volder, S. H. Tawfick, R. H. Baughman and A. J. Hart, *Science*, 2013, 339, 535-539.
84. M. Ratner, *Nature Nano*, 2013, 8, 378-381.
85. E. Masliah, E. Rockenstein, I. Veinbergs, Y. Sagara, M. Mallory, M. Hashimoto and L. Mucke, *Proceedings of the National Academy of Sciences of the United States of America*, 2001, 98, 12245-12250.
86. D. J. Irwin, V. M. Y. Lee and J. Q. Trojanowski, *Nature Reviews Neuroscience*, 2013, 14, 626-636.

Soft Matter Accepted Manuscript

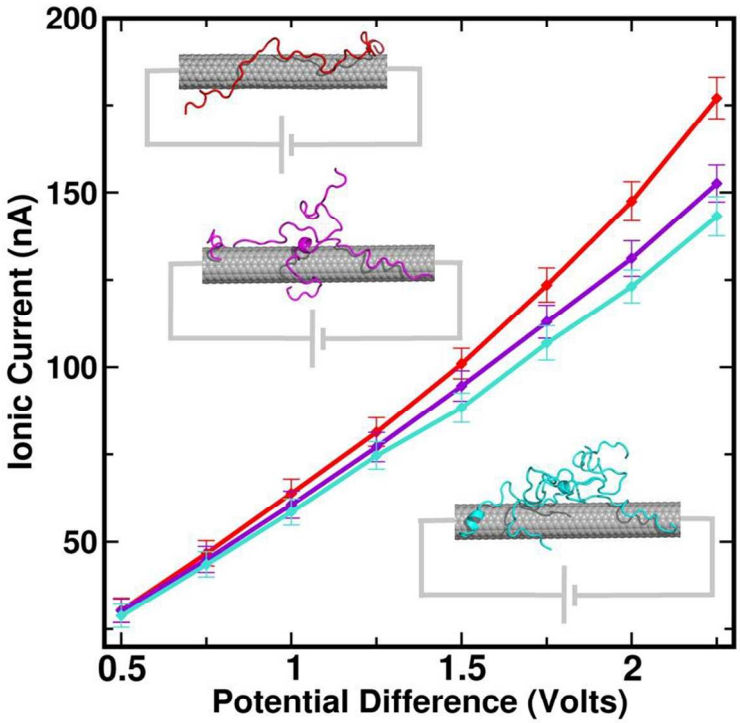

Electrical current signals of SWCNT adsorbed full-length Aβ contain information about the oligomeric state.
203x175mm (150 x 150 DPI)

Soft Matter Accepted Manuscript